0026-895X/87/040392-09$02.00/0

MOLECULAR PHARMACOLOGY, 31:392–400

Kinetics and Mechanism of L-[^{3}H]Nicotine Binding to Putative High Affinity Receptor Sites in Rat Brain

PATRICK M. LIPPIELLO, STEPHEN B. SEARS, and KAY G. FERNANDES

Research and Development, Bowman Gray Technical Center, R. J. Reynolds Tobacco Company, Winston-Salem, North Carolina 27102

Received October 29, 1986; Accepted January 27, 1987

SUMMARY

The properties of high affinity nicotine-binding sites in rat brain were studied by monitoring the kinetics of L-[^{3}H]nicotine binding to whole brain membrane preparations, including both total membranes and membrane subfractions. Although nicotine appeared to bind to a single class of sites, with an apparent equilibrium dissociation constant of 2–3 nM, the binding kinetics were biphasic at all temperatures and at all nicotine concentrations tested. An initial rapid binding process, with an association rate constant of around 0.02 min^{-1} nM^{-1} at 0°, was followed by a slower binding process. Both the rate and the proportion of binding that occurred by the slower process were dependent on the nicotine concentration. By comparison, the kinetics of dissociation were first order at all concentrations, with a rate constant of 0.04 min^{-1} at 0° The rates of both association and dissociation increased significantly with temperature, but there was no change in the apparent affinity of the sites. The same results were obtained with several different membrane preparations, including whole brain membrane preparations, detergent-permeabilized membranes, P-2 fractions, and synaptosomes. The results were found to be consistent with a two-state model. Analyses based on this model indicate that the binding sites can assume two different conformations, one having a high affinity (K_D = 1 nM) and the other a low affinity (K_D = 150 nM) for nicotine. It was estimated that approximately 60% of the sites are in the low affinity conformation in the absence of ligand. However, the evidence suggests that nicotine binding can facilitate a shift in the conformational equilibrium, favoring the high affinity state.

Although nicotinic cholinergic receptors at the mammalian neuromuscular junction have been thoroughly characterized (1–4), much less is known about the nature of nicotinic receptors in the brain. Putative receptors in the brain were originally identified by their ability to bind α-bungarotoxin (5), a potent nicotinic cholinergic antagonist at the neuromuscular junction. However, the functional significance of α-bungarotoxin-binding sites is not clear because attempts to block neural transmission with this ligand have been unsuccessful (6–8).

More recently, equilibrium binding studies have revealed sites in the brain that bind nicotinic agonists, such as acetylcholine (9) and nicotine (10–12), with high affinity. The binding properties of these sites, as well as their regional distribution in the brain, are clearly different from those of the toxin-binding sites (10, 13). Moreover, high affinity agonist-binding sites can be solubilized and separated chromatographically from the α-bungarotoxin binding component (14, 15), indicating that the two reside on distinct molecules.

The high affinity binding components identified by nicotine and acetylcholine share many common features. For example, the equilibrium binding properties of sites labeled by [^{3}H]acetylcholine and [^{3}H]nicotine, including the apparent affinity and the maximum number of sites, are essentially the same (16, 17). The binding of both ligands is effectively inhibited by nicotinic cholinergic agonists (9, 18), and the regional distributions of nicotine- and acetylcholine-binding sites in the brain, determined autoradiographically, are similar, if not identical (13). In addition, chronic nicotine administration *in vivo* results in the up-regulation of both [^{3}H]acetylcholine and [^{3}H]nicotine binding (19, 20). There is also evidence from lesioning studies that in some parts of the brain the sites labeled by both agonists are located presynaptically on catecholamine axons (21, 22). It has been suggested that these sites may play a neuromodulatory role by controlling neurotransmitter release (23). Based on these lines of evidence it seems likely that the sites labeled by acetylcholine and nicotine represent a unique class of nicotinic cholinergic receptors in the brain.

It has been suggested that high affinity agonist-binding sites in the brain may be related to nicotinic receptors present at autonomic ganglia (18). This hypothesis is based on the fact that the most effective competitive inhibitors at these sites are also potent ganglionic agonists. However, several anomalies demand explanation. For example, in view of the relatively high agonist concentrations that are necessary to elicit ganglionic responses *in vivo* (24), the significance of the high affinity binding observed *in vitro* must be questioned. This, together

ABBREVIATIONS: EDTA, ethylenediaminetetracetic acid; PMSF, phenylmethylsulfonyl fluoride; Hepes, 4-(2-hydroxyethyl)-1-piperazineethanesulfonic acid.

with the fact that classical nicotinic antagonists are poor competitive inhibitors of nicotine and acetylcholine binding, has led some investigators to hypothesize either that high affinity sites labeled by nicotinic agonists are substantially different from peripheral nicotinic receptors (18), or that they are noncholinergic (25). A possible explanation that has been offered for these anomalies is that the equilibrium binding properties determined *in vitro* reflect the conversion of low affinity sites to a high affinity, agonist-selective state (18).

If conversion from a low affinity to a high affinity state occurs, it is reasonable to suspect that it would be observable kinetically. Interconversion of receptor conformers has, in fact, been reported for other cholinergic systems, including muscarinic receptors in chick heart (26) and nicotinic receptors from *Electrophorus* (27) and *Torpedo* (28) electric tissue. Such conformational transitions are characterized by complex binding kinetics and have been related to the process of receptor desensitization *in vivo* (28). We previously observed that the binding of L-[^{3}H]nicotine to rat brain membranes exhibited complex kinetics, not explainable by multiple binding sites (12). These studies have now been extended in order to define a model that adequately describes the kinetics of nicotine binding to high affinity sites *in vitro*. The results indicate that a two-state model, based on a single class of sites that can assume either a low affinity or a high affinity conformation, is sufficient to account for the binding kinetics. Since this model predicts that nicotine will stabilize the high affinity conformer, it is consistent with the fact that a single class of high affinity sites is observed at equilibrium.

Materials and Methods

Animals. Female Sprague-Dawley rats (100–200 g) were purchased from the Harlan Co. (Indianapolis, IN). Animals were housed separately in hanging stainless steel wire cages and were maintained on a 12-hr light/dark cycle (7 a.m.–7 p.m.). They received standard Purina Rat Chow (No. 5001) and water *ad libitum*.

Tissue preparation. Rats were anesthetized with 70% CO_2 prior to killing by decapitation. Whole brains were removed, rinsed with ice-cold buffer, and homogenized at 0–4° in 10 volumes of buffer (w/v) using a Brinkmann Polytron, setting 6, for 10 sec. The preparative buffer consisted of Na_2HPO_4, 8 mM; KH_2PO_4, 1.5 mM; KCl, 3 mM; NaCl, 120 mM; EDTA, 2 mM; Hepes, 20 mM; iodoacetamide, 5 mM; and PMSF, 0.1 mM (pH 7.4 at 0°). The inclusion of protease inhibitors was necessary to avoid possible binding artifacts, based on previous studies (12). The homogenate was sedimented by centrifugation (50,000 × *g*, 20 min, 0°). The pellet was resuspended in distilled, deionized water, (5%, w/v) and incubated for 1 hr on ice. Membranes were recovered by centrifugation as above, and resuspended in the assay buffer at a concentration of around 1 mg of protein/ml. The composition of the standard assay buffer was the same as the preparative buffer, with the addition of $MgCl_2$, 1 mM, and $CaCl_2$, 2 mM, and the elimination of EDTA, iodoacetamide, and PMSF.

For experiments that utilized subfractionated membranes, P-2 fractions (i.e., myelin, membrane fragments, synaptosomes, and mitochondria) and synaptosomal fractions were prepared and characterized according to previously described methods (29). In all preparations, the initial homogenization step was carried out in the presence of EDTA, PMSF, and iodoacetamide, as above. After recovery of P-2 and synaptosomal fractions, the membranes were resuspended in distilled, deionized water (5%, w/v), and incubated for 1 hr on ice. Membranes were then recovered by centrifugation, as above, and resuspended in the standard assay buffer.

For experiments utilizing permeabilized preparations, unfractionated membranes were prepared from whole brain and resuspended in assay buffer containing 0.5 mg/ml saponin for 1 hr on ice before being used in incubations. This concentration of detergent was sufficient to permeabilize the membranes (30) but did not reduce net specific binding.

For all membrane preparations, protein was determined according to the method of Lowry *et al.* (31).

Equilibrium binding assays. The assay mixture typically consisted of 0.2–0.4 mg of membrane protein in a final incubation volume of 0.5 ml. The concentration of nicotine was varied from 0.1 to 200 nM, using only L-[^{3}H]nicotine. Incubations were performed at 0° for 2 hr in a temperature-controlled cryobath (Exacal Ex-700). Assays were initiated by addition of the membrane suspension with rapid mixing. Blank incubations contained 100 μM L-nicotine salicylate. Incubations were terminated by adding 5 ml of ice-cold assay buffer, followed by rapid filtration under vacuum through a double thickness of Gelman type A/E glass fiber filters (pore size 0.3 μm), using a Brandel multi-manifold tissue harvester. Filters were presoaked in 0.1% poly-L-lysine at 4°, to reduce nonspecific binding (18). Following the initial filtration, filters were washed three times with cold assay buffer containing 0.1% poly-L-lysine (5 ml each) and air dried. Filters were then placed in counting vials and mixed vigorously with 20 ml of liquid scintillation fluid (Scinti-Verse II, Fisher Scientific Co.), before quantification of radioactivity. Samples were counted in a Beckman LS-7000 liquid scintillation counter at 50% efficiency. All determinations were in triplicate. Specific binding to membranes was determined as the difference in binding between samples containing unlabeled L-nicotine salicylate (100 μM) and those which contained none. Equilibrium binding data were analyzed using an iterative least squares algorithm called LIGAND (32), on an HP-86 microcomputer.

Binding kinetics. The time course of nicotine binding was determined by incubating fixed concentrations of L-[^{3}H]nicotine (1, 2, 5, 10, 30, 50, 100, and 200 nM) with 0.25 mg of membrane protein for varying amounts of time at 0°, 22°, or 37°. Incubations were terminated at successive time points by rapid filtration, as described above. The dissociation kinetics were followed by first incubating a fixed concentration of radiolabeled nicotine with 0.25 mg of membrane protein, until equilibrium was achieved, at 0° (2 hr), 22° (20 min), or 37° (5 min). This incubation was followed by isotopic dilution with an excess of unlabeled nicotine salicylate (1 mM), or by volumetric dilution (1:50) with assay buffer. Samples were rapidly filtered at successive times thereafter, followed by quantification of bound radioactivity. For each time point total binding and blanks were determined in triplicate.

Kinetic analyses. The kinetic analyses in the present studies were based on an exact (linear) solution to the differential equations for the cyclic model of receptor desensitization originally proposed by Katz and Thesleff (33), assuming buffered ligand concentrations (see Results for detailed mechanism). This assumption was considered reasonable since the concentration of sites (ca. 0.05–0.1 nM) was well below the apparent K_D and the concentrations of ligands were always 10- to 2,000-fold higher. The concentration of receptor species as a function of time can be expressed as follows:

$$C_R(t) = \sum_{j=1}^{4} X_j \cdot Y_{1j} \cdot e^{-z_j t} \quad (1)$$

$$C_{RL}(t) = \sum_{j=1}^{4} X_j \cdot Y_{2j} \cdot e^{-z_j t} \quad (2)$$

$$C_{R'}(t) = \sum_{j=1}^{4} X_j \cdot Y_{3j} \cdot e^{-z_j t} \quad (3)$$

$$C'_{RL}(t) = \sum_{j=1}^{4} X_j \cdot Y_{4j} \cdot e^{-z_j t} \quad (4)$$

where $C(t)$ represents the concentrations of the unliganded (R, R') and liganded (RL, $R'L$) forms of the low and high affinity states, respectively. The X_j are functions of Y_{ij} as follows:

$$X_j = [\mathrm{Det}(Y)]j/\mathrm{Det}(Y) \quad j = 1, 2, 3, 4, \tag{5}$$

where

$$\mathrm{Det}(Y) = \begin{vmatrix} 1 & 1 & 1 & 1 \\ Y_{21} & Y_{22} & Y_{23} & Y_{24} \\ Y_{31} & Y_{32} & Y_{33} & Y_{34} \\ Y_{41} & Y_{42} & Y_{43} & Y_{44} \end{vmatrix}$$

and $[\mathrm{Det}(Y)]j = \mathrm{Det}(Y)$ with the jth column replaced by the initial concentrations of the four species, $C_R(O)$, $C_{RL}(O)$, $C_R'(O)$, and $C_{RL}'(O)$.

For $j = 1, 2, 3, 4$, the Y_{ij} in $\mathrm{Det}(Y)$ are functions of Zj and the eight rate constants that define the model ($k_1 \ldots k_8$) as follows:

$$Y_{1j} = 1 \tag{6}$$

$$Y_{2j} = (k_1k_8(S_3 - Z_j) + k_4k_5(S_1 - Z_j))/D_j \tag{7}$$

$$Y_{3j} = (k_1k_3k_8 - k_1k_2k_8 + k_8(S_1 - Z_j)(S_2 - Z_j))/D_j \tag{8}$$

$$Y_{4j} = ((S_1 - Z_j)(S_2 - Z_j)(S_3 - Z_j) - k_3k_4(S_1 - Z_j) - k_1k_2(S_3 - Z_j))/D_j \tag{9}$$

where $S_1 = k_1 + k_7$, $S_2 = k_2 + k_3$, $S_3 = k_4 + k_8$, $S_4 = k_5 + k_8$, $D_j = k_8(S_2 - Z_j)(S_3 - Z_j) + k_2k_4k_8 - k_3k_4k_8$, and k_1, k_5 are pseudo-first order rate constants.

The exponential coefficients (Z_j) can be expressed as follows:

$$Z_1 = 0 \tag{10}$$

$$Z_2 = 2(-a/3)^{1/2}\mathrm{COS}(Q/3) + A/3 \tag{11}$$

$$Z_3 = 2(-a/3)^{1/2}\mathrm{COS}(Q/3 + 2\pi/3) + A/3 \tag{12}$$

$$Z_4 = 2(-a/3)^{1/2}\mathrm{COS}(Q/3 + 4\pi/3) + A/3 \tag{13}$$

where $\mathrm{COS}(Q) = (-b/2)/(-a^3/27)^{1/2}$, $a = (3B - A^2)/3$, $b = (-2A^3 + 9AB - 27C)/27$, and

$$A = k_1 + k_2 + k_3 + k_4 + k_5 + k_6 + k_7 + k_8$$

$$B = k_1(k_3 + k_5) + (k_2 + k_3)(k_5 + k_7) + k_5k_7 + k_4(k_1 + k_2 + k_5 + k_7) + k_6(k_1 + k_2 + k_3 + k_7) + k_8(k_1 + k_2 + k_3 + k_4 + k_6)$$

$$C = k_1k_3k_5 + k_2k_5k_7 + k_3k_5k_7 + k_4(k_2k_5 + k_2k_7 + k_1k_5 + k_5k_7) + k_6(k_2k_7 + k_1k_3 + k_3k_7) + k_8(k_2k_6 + k_1k_6 + k_3k_6 + k_2k_4 + k_1k_4 + k_1k_3)$$

The equilibrium dissociation constant can be expressed as a function of the rate constants, as follows:

$$K_{eq} = (k_2k_6k_7 + k_2k_6k_8)/(k_2k_5k_7 + k_1k_6k_8)$$

This model was adapted to an HP-86 microcomputer and manual iterative curve-fitting procedures were carried out by varying the rate constants within experimentally determined limits. Parameter estimates were obtained either experimentally or by manual iterative curve-fitting and confirmed by statistical curve-fitting analyses on individual data sets, using PCNONLIN (Statistical Consultants Inc., Lexington, KY) (see Results).

Materials. The following chemicals were obtained from Sigma Chemical Co. (St. Louis, MO): poly-L-lysine hydrobromide, iodoacetamide, PMSF, and saponin. The salicylate salt of L-nicotine was prepared by standard methods (34) and recrystallized from alcohol. L-[^{3}H]nicotine (*N-methyl*-[^{3}H], specific activity 75.7 Ci/mmol or 60.4 Ci/mmol), purity > 99%, was obtained from New England Nuclear Corp. (Newton, MA) and stored at −20° in an ethanol solution. Glass fiber filters, Gelman type A/E, were purchased from American Scientific Products (McGraw Park, IL). All other chemicals were of the highest grade commercially available.

Results

Equilibrium binding. To assess the number of classes of nicotinic sites present in membrane preparations, the equilibrium binding of L-[^{3}H]nicotine was monitored, using a rapid filtration method previously described (12, 18). A Scatchard analysis of the data from several experiments is presented in Fig. 1. A single class of high affinity binding sites was consistently observed. These sites were saturable over the concentration range 1–200 nM and had an apparent affinity (K_d) for nicotine of 2–3 nM. The maximum number of sites was estimated to be around 200 fmol/mg of membrane protein. A more detailed description of the equilibrium binding properties of these sites has been presented elsewhere (12).

Association kinetics. To obtain a detailed picture of the association kinetics, the time course of nicotine binding was followed. The time resolution achievable with the rapid filtration method was around ±15 sec. Initial experiments utilized a nicotine concentration equivalent to the equilibrium dissociation constant (2 nM). At this concentration nonspecific tissue binding was less than 5% of the total and did not change with time. The results indicated that nicotine binding was biphasic (Fig. 2A). A rapid binding phase, characterized by a pseudo-first order rate constant (k_{ob}) of 0.08 min^{-1}, was followed by a second binding process that was roughly 5 times slower. At this concentration of nicotine (2 nM) the fast phase binding appeared to be complete in 20 min (Fig. 2A, *inset*). The slower process continued until equilibrium was reached, at approximately 3 hr. The relative contributions of the fast (B_f) and slow (B_s) binding components were estimated by linear regression of the slow phase portion of the semilog plot (Fig. 2A, *inset*) and extrapolation to zero time. At 2 nM nicotine about 40% of the total binding was accounted for by the slow binding process. By difference, 60% was attributable to the rapid binding process.

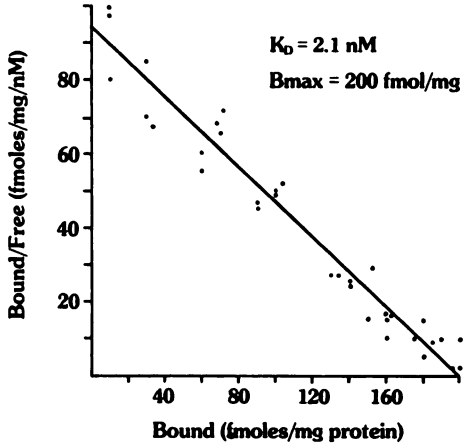

Fig. 1. Equilibrium binding of L-[^{3}H]nicotine to rat brain membranes. Membranes were isolated from adult female brain tissue, as described under Materials and Methods, and 0.20–0.40 mg of membrane protein were incubated with varying amounts of radiolabeled nicotine (0.1–200 nM) in a total volume of 0.5 ml for 2 hr at 0°. Nonspecific binding was determined from blank incubations that contained 100 μM L-nicotine salicylate. The data shown represent the combined results from five separate binding experiments, each done in triplicate. Scatchard analysis was performed using a computerized method (LIGAND) previously described (32).

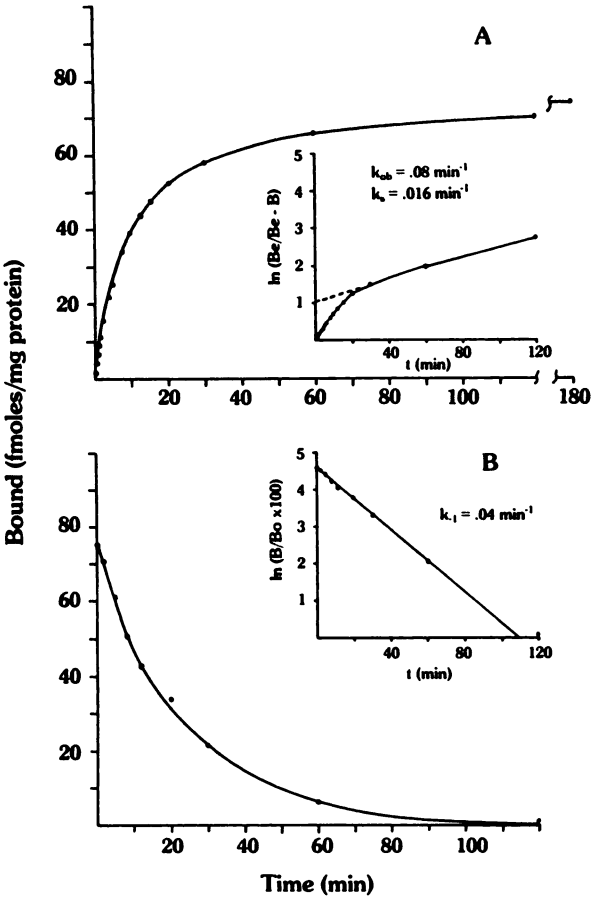

Fig. 2. Kinetics of L-[^{3}H]nicotine binding to rat brain membranes. Membranes isolated from whole brain (0.25 mg of protein) were incubated with 2 nM radiolabeled nicotine for varying amounts of time (0–3 hr) at 0° in a total volume of 0.5 ml. The amount of specific binding was determined at each time by rapid filtration, as described in the text. Blank incubations contained 100 μM L-nicotine salicylate. The results shown are representative of four separate experiments, done in triplicate. A. Association kinetics. The association rate constant (k_{ob}) was estimated from the initial slope of the semilog plot (*inset*) and the isomerization rate constant (k_s) was determined from the slope of the slow phase binding component (20 min–3 hr), by linear regression. B. Dissociation kinetics. Membranes were incubated for 2–3 hr and then dissociation was initiated by the addition of excess unlabeled L-nicotine salicylate (1 mM). The dissociation rate constant (k_{-1}) was determined from the slope of the semilog plot (*inset*).

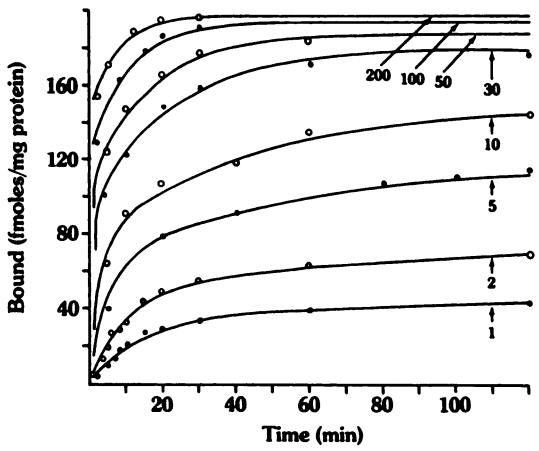

Fig. 3. Concentration dependence of binding kinetics. The time course of L-[^{3}H]nicotine binding to rat brain membranes was determined, as described under Materials and Methods. Varying amounts of radiolabeled nicotine (1–200 nM) were incubated with 0.25 mg of membrane protein at 0°, for up to 2 hr. The results shown are representative of at least three experiments, done in triplicate, at each concentration. The theoretical curves were determined by iterative curve-fitting using the two-state model described in the text.

Dissociation kinetics. The dissociation kinetics were monitored by isotopic dilution with excess unlabeled nicotine. In contrast to association, the dissociation of bound nicotine occurred by a first order process (Fig. 2B). For membranes equilibrated with 2 nM L-[^{3}H]nicotine, the off-rate (k_{-1}) was 0.04 min^{-1} and dissociation was essentially complete in 2 hr. The equilibrium dissociation constant, calculated from the kinetic data ($K_d = k - 1/((k_{ob} - k_{-1})/[\text{nicotine}])$, was 2 nM, in very good agreement with the value determined from equilibrium binding studies.

Concentration dependence of kinetics. To evaluate possible mechanisms that could account for the observed kinetics, the concentration dependence of association and dissociation was determined. The time course of [^{3}H]nicotine binding was monitored for nicotine concentrations ranging from 1 to 200 nM. The results of several experiments are presented in Fig. 3. The curves shown are theoretical and were fitted to the data using a two-state model, which will be described in more detail in a subsequent section. To analyze the fast and slow phase binding components at each concentration, the data were plotted on a semilog scale, as before (Fig. 4). The data illustrate several important points. First, the contribution of the slow phase process to total binding, estimated by extrapolation of the curves to zero time, increased from around 30% at 1 nM nicotine to 60% at 30 nM. However, at higher concentrations the amount of slow phase binding actually decreased, accounting for 25% of the binding at 200 nM nicotine. By comparison, the rate of slow phase binding, as judged by the slopes of the slow phase components in Fig. 4, was essentially unchanged at lower nicotine concentrations (1–10 nM) but did increase significantly at higher concentrations (30–200 nM).

The rate of dissociation of bound ligand was also determined, following equilibration of membranes with several concentrations of L-[^{3}H]nicotine, using either isotopic dilution with excess (1 mM) unlabeled L-nicotine or volumetric dilution (1:50) with assay buffer. The results are shown in Fig. 5. In experiments based on isotopic dilution, dissociation was found to be first order at all concentrations tested, with a rate constant (k_{-1}) of 0.04 min^{-1}. In experiments based on volumetric dilution, dissociation was first order over the first 10 min (Fig. 5, *inset*). Thereafter, the rate of dissociation decreased as binding approached the new (non-zero) equilibrium point. When the data were corrected for this decrease by subtracting the predicted equilibrium binding value, dissociation was first order over the first 90 min. The dissociation rate constant was 0.04 min^{-1}, in good agreement with isotopic dilution experiments. In some experiments dissociation was followed after incubating membranes with radiolabeled nicotine for only 2 min. The rate of dissociation was the same as before (Fig. 5, *inset*). However, the curves consistently intersected the y axis [i.e., $\ln(B/B_m)$] at a point lower than the value actually measured prior to isotopic dilution. Therefore, at the earliest time point, which represents the time required for the addition of unlabeled nicotine and immediate filtration (ca. 10–15 sec), there was evidence of a rapid decrease in binding. Again, this decrease was significant

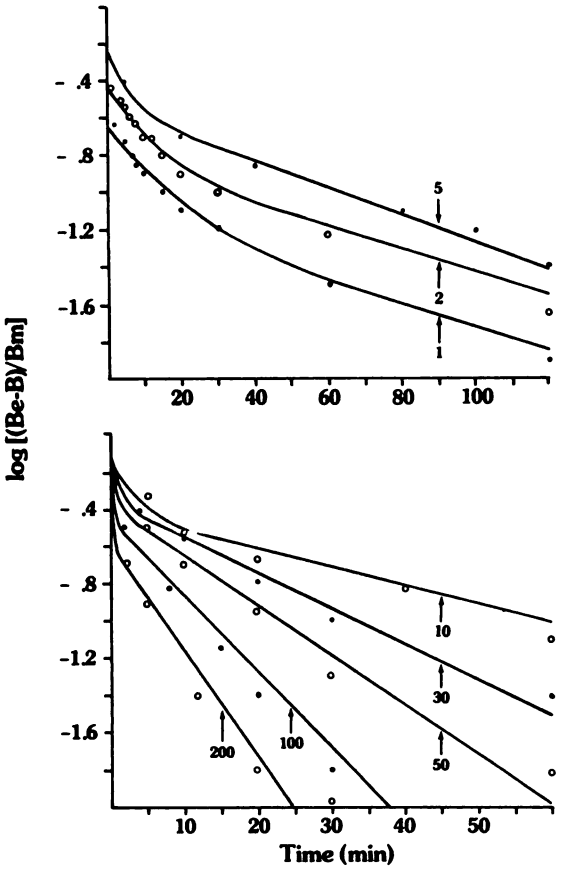

Fig. 4. Concentration dependence of fast and slow phase binding components. The data of Fig. 3 were plotted as log $[(B_e - B)/B_m]$ versus time for each concentration of nicotine, where B is the amount bound at time t, B_m is the maximal number of sites (B_{max}) present in the membranes, and B_e is the amount of nicotine bound at equilibrium for each concentration, determined from double reciprocal analysis of the data of Fig. 3. The theoretical curves were determined by iterative curve-fitting, using a two-state model.

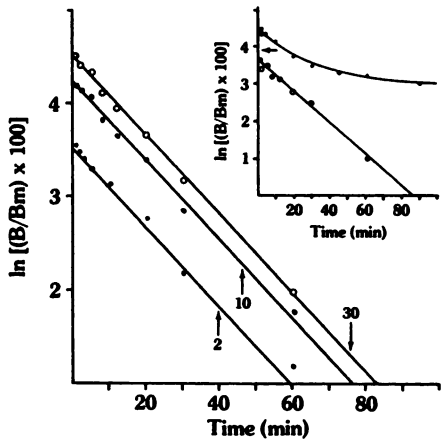

Fig. 5. Dissociation kinetics of bound L-[^{3}H]nicotine. Membranes were isolated from whole brain, as described in the text, and several concentrations of radiolabeled nicotine (2, 10, and 30 nM) were incubated with 0.25 mg of protein at 0° until equilibrium was achieved (2–3 hr). Dissociation was followed after the addition of excess unlabeled L-nicotine salicylate (1 mM). *Inset*: Dissociation was followed by isotopic dilution, as above, after a 2-min incubation of membranes with 3 nM radiolabeled nicotine (i.e., non-equilibrium binding; ○); ←, the amount of binding prior to the addition of unlabeled nicotine. Dissociation was also monitored by incubating membranes with 30 nM radiolabeled nicotine for 2 hr, followed by volumetric dilution (1:50) with assay buffer (●).

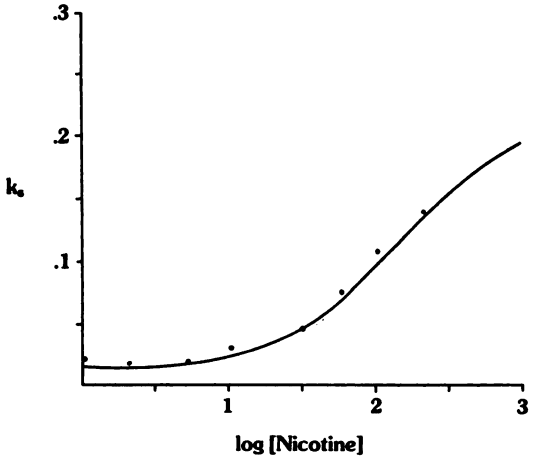

Fig. 6. Concentration dependence of the rate of slow phase binding. The isomerization rate constant (k_e) was estimated for each nicotine concentration from the slopes of the slow phase binding compounds (Fig. 4), as described in the text. Values were plotted as a function of nicotine concentration. The theoretical curve was constructed using an analytical solution for k_e, previously derived for a two-state model (35).

in terms of evaluating possible kinetic models (see below), since it suggested the presence of a low affinity binding component under nonequilibrium conditions.

The rate of the slow binding process (k_e) was estimated at several different nicotine concentrations (1–200 nM) from the slopes of the slow phase binding components of Fig. 4. Between 1 and 10 nM nicotine the rate of slow phase binding was relatively insensitive to changes in ligand concentration (Fig. 6). However, k_e increased approximately 6-fold between 10 and 200 nM. This increase is characteristic of a two-state mechanism (28).

The contribution of the rapid binding process was also determined as a function of nicotine concentration, from the data of Fig. 4. The amount of binding attributable to the fast phase component (B_f) was estimated from $B_e - B_s$, where B_s is the amount of slow phase binding determined from linear extrapolation of the slow phase component to zero time, and B_e is the total amount bound at equilibrium for each nicotine concentration. The concentration dependence of B_f was biphasic (Fig. 7). This result is also relevant to the kinetic mechanism since it implies that the rapid initial binding process reflects the interaction of nicotine with two sites of different affinity. The affinities of the two sites for nicotine were estimated from the slopes of the two components of Fig. 7. The apparent dissociation constants indicated a high affinity component with a K_d of around 1 nM and a low affinity component with a K_d of 150 nM.

Kinetic mechanism. The basic observations of biphasic association kinetics, first order dissociation kinetics, the concentration dependence of the rate of slow phase binding (k_e), and the concentration dependence of the rapid binding component (B_f) are all characteristic of a two-state mechanism (28). Therefore, the results were analyzed according to the following model, which is the simplest one that adequately accounts for all of the data.

This model assumes a homogeneous population of binding sites that can exist in either of two conformations in the absence of ligand, one having a low affinity (R) and the other a high affinity (R') for nicotine (N). This model is described

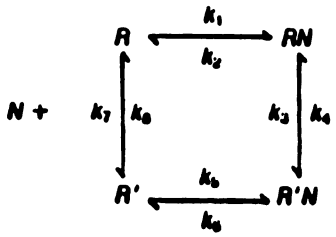

by eight rate constants ($k_1 \ldots k_8$) and four equilibrium constants ($K_1 \ldots K_4$), where $K_1 = k_2/k_1$, $K_2 = k_4/k_3$, etc. For a cycle such as this, knowledge of any three equilibrium constants determines the fourth, where $K_1 = K_3 \cdot K_4/K_2$.

The biphasic association kinetics (Figs. 2 and 3) result from the rapid (diffusion-controlled) binding of nicotine to R and R' which is followed by a second binding phase governed by the relatively slower isomerizations between pairs of receptor conformers (i.e., $R \leftrightarrow R'$ and $RN \leftrightarrow R'N$). The slope of the slow phase binding component (k_s) is a measure of the overall isomerization rate. An analytic expression has been previously derived for k_s (35) showing that it reaches limiting values of $k_7 + k_8$ at low ligand concentrations and $k_3 + k_4$ at high concentrations, and is equal to $k_4 + k_7$ at intermediate concentrations, thus accounting for the "sigmoidal" shape of Fig. 6. The model also predicts that the concentration dependence of fast phase binding (B_f) should be biphasic (as in Fig. 7), reflecting the rapid initial interaction of nicotine with R and R', each of which has a different affinity for the ligand. If the affinity of $R' \gg R$, the binding of the ligand tends to stabilize $R'N$ at equilibrium. This would account for the apparent binding of nicotine to a single class of high affinity sites in equilibrium binding studies (Fig. 1). In addition, since $R'N$ is the predominant species at equilibrium, the off-rate (k_{-1}) is determined primarily by k_6 ($R'N \rightarrow R' + N$), resulting in apparent first order dissociation kinetics (Fig. 5). This rate was found to be independent of the concentrations of nicotine with which the membranes were initially equilibrated, a specific prediction of the two-state model (see Fig. 5).

Kinetic analyses. The ability of the two-state mechanism to account for the observed kinetics was further evaluated by deriving an exact analytic solution to the model, assuming buffered ligand concentrations throughout (see Materials and Methods). This solution was adapted to a microcomputer for estimation of the kinetic parameters by iterative curve-fitting. Initial estimates of the kinetic parameters were determined from the experimental data as follows. The equilibrium dissociation constants, K_1 and K_3, were determined graphically from the slopes of the two binding components of B_f (Fig. 7). Similarly, the fraction of sites represented by the high affinity conformer was estimated from Scatchard analysis of the data of Fig. 7 using a two-site fit, giving a value of 40%. From this information K_4 could be calculated, and in turn, $K_2 = K_3 \cdot K_4/K_1$. The four equilibrium constants were also constrained to yield the independently determined equilibrium dissociation constant (K_{eq}), where $K_{eq} = K_3(1 + K_4)/(1 + (K_3/K_1)K_4)$.

Initial values for six of the eight rate constants were estimated by similar methods. Specifically, k_5 was estimated from the initial slope of the association kinetics (Fig. 2) since at early times the ligand binds primarily to the high affinity conformer. The on-rate for binding to the low affinity conformer (k_1) was initially estimated to be approximately the same as k_5, but was varied independently during the curve-fitting procedure (see Table 1). By this model the dissociation rate constant (k_{-1}) is a measure of k_6, and k_2 can be calculated from $k_1 \cdot K_1$. Initial values for k_7 and k_8 were determined from the relationship $K_4 = k_8/k_7$ and the limiting value of k_s ($= k_7 + k_8$) at low ligand concentrations (Fig. 6). The ratio of k_4/k_3 was obtained from K_2. However, since k_s could not be determined at high enough ligand concentrations to measure the limiting value of $k_3 + k_4$ (Fig. 4), these two parameters were varied during iterative curve-fitting procedures to obtain estimates.

The results of manual iterative curve-fitting procedures yielded the theoretical curves of Figs. 3–7. The parameter estimates are shown in Table 1. These estimates agreed well with statistical curve-fitting analyses of individual data sets also shown in Table 1. Dissociation curves were also computer-generated, by setting the initial values of R, R', RN, and $R'N$

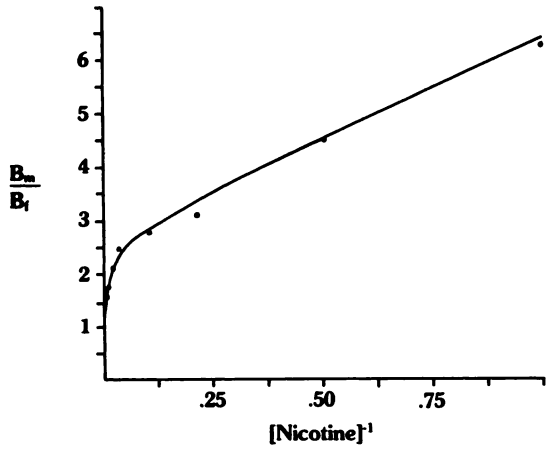

Fig. 7. Concentration dependence of fast phase binding. The contribution of the rapid binding process (B_f) to total binding was determined for several nicotine concentrations, from the data of Fig. 4, as described in the text. The theoretical curve was generated by iterative curve-fitting, based on a two-state model.

TABLE 1
Equilibrium and kinetic constants for ^{3}H-L-nicotine binding

Binding parameters	Method of initial estimation	Parameter estimates	
		Experimental[a]	Statistical[b]
K_{eq} (nM)	Equilibrium binding	3.3	
K_1 (nM)	Concentration dependence of B_f (Fig. 7)	150	
K_2	$K_2 = K_3 \cdot K_4/K_1$	0.013	
K_3 (nM)	$K_3 = k_6/k_5$	1.3	1.0
K_4	Concentration dependence of B_f (Fig. 7)	1.5	
k_1 (nM^{-1} min^{-1})	Assume $k_1 \simeq k_5$	0.03	0.02
k_2 (min^{-1})	$k_2 = k_1 \cdot K_1$	4.5	7.5
k_3 (min^{-1})	Concentration dependence of k_s (Fig. 6)	0.22	0.30
k_4 (min^{-1})	$k_4 = K_2 \cdot k_3$	0.003	0.0025
k_5 (nM^{-1} min^{-1})	Slope of rapid binding component (Fig. 2A)	0.03	0.04
k_6 (min^{-1})	Dissociation constant (k_{-1})	0.04	0.04
k_7 (min^{-1})	Concentration dependence of k_s ($=k_7 + k_8$)	0.006	0.006
k_8 (min^{-1})	and $k_8 = K_4 \cdot k_7$	0.009	0.009

[a] Parameter estimates were obtained by manual iterative curve-fitting of the association and dissociation kinetic data for all nicotine concentrations as described in the text.

[b] Individual data sets were also fitted using a nonlinear least squares algorithm (PCNONLIN) to obtain estimates for the rate constants. The data shown are for [nicotine] = 2 nM (average of six separate experiments done in triplicate).

to their equilibrium values for a given nicotine concentration (N) and then decreasing the value of N 1000-fold, thus simulating a volumetric dilution experiment. Final parameter estimates for the model are reported in Table 1. These parameters yielded an acceptable fit to all of the data within experimental error (±5%).

Effects of membrane properties and temperature. Since the initial experiments were all based on total brain membrane preparations it was important to determine whether the heterogeneity of the membranes or membrane physical properties were a factor in determining the kinetics of binding. The results of several control experiments are shown in Table 2. It was found that the rate constants for association, dissociation, and isomerization were essentially the same for whole brain membrane preparations and for the more purified P-2 and synaptosomal fractions. To eliminate the further possibility that rate-limiting diffusion barriers might be present in these preparations, membranes were permeabilized with saponin (30) prior to being utilized in kinetics experiments. The results were unchanged (Table 2).

In order to determine the effects of temperature, binding experiments were also performed at 0°, 22°, and 37°. Binding was biphasic at all temperatures, and dissociation was first order (Table 3). There was a substantial increase in the rate constants for association, dissociation, and isomerization as expected, but the apparent equilibrium dissociation constant, calculated from these data, was the same at all temperatures. Therefore, the binding properties of the sites were not appreciably affected by changes in temperature over this range.

Discussion

In order to reconcile the high affinity binding properties of nicotinic binding sites *in vitro* with the relatively high concentrations of ligand needed to elicit a physiological response, Romano and Goldstein (18) proposed that the equilibrium binding properties of the sites reflected their conversion to a high affinity, agonist selective, state. Although the present results do not address the issue of selectivity, they do support the notion that the high affinity binding of L-[^{3}H]nicotine to putative receptor sites in rat brain tissue results from agonist-induced conformational changes. These changes are best described by a two-state model. This conclusion is supported by the detailed kinetic analyses as well as by the consistency of the results with specific predictions of the model, including biphasic association kinetics, first-order dissociation kinetics, a relatively invariant isomerization rate constant (k_e) at low ligand concentrations, biphasic dependence of the rapid binding process on ligand concentration, lack of dependence of the dissociation rate on initial ligand concentration, and a small, rapidly dissociating binding component following brief incubations with the ligand.

The following alternative models were also considered but were found to be unsuitable since none could account for all of the experimental observations, and the data could not be fit to exact integrated solutions to the models for any choice of kinetic parameters.

$$R + N \leftrightarrow RN \qquad R' + N \leftrightarrow R'N \tag{1A}$$

$$R + N \leftrightarrow RN \leftrightarrow R'N \tag{2A}$$

$$Ra + N \leftrightarrow RaN \qquad Rb + N \leftrightarrow RbN \leftrightarrow Rb'N \tag{3A}$$

Model 1A assumes two independent binding sites with different affinities for the ligand (N). This model is clearly inconsistent with the results of equilibrium binding studies (Fig. 1). In addition, such a model does not predict a change in the proportion of rapidly reacting sites with increasing ligand concentrations. Model 2A is based on the rapid initial binding of the ligand to a low affinity site (RN) which is then converted to a high affinity conformation ($R'N$). This model was suggested by Galper *et al.* (26) to account for the binding of quinuclidinyl benzilate to muscarinic receptors. However, several predictions of this model are inconsistent with the present data. For example, since the affinity of $R \ll R'$, the binding that occurs during brief exposure to the ligand would be almost exclusively to the low affinity conformer (RN). As a result, dissociation should be more rapid under these conditions than it is following complete equilibration (i.e., when $R'N \rightarrow RN$ is rate-limiting). However, our findings indicate that the rate of dissociation is the same under all conditions. This model also predicts that the proportion of total binding attributable to the rapid process should increase with ligand concentration, whereas the opposite was actually observed for nicotine binding. Model 3A assumes two classes of sites, one having high affinity (Ra) and the other low affinity (Rb) for the ligand, and binding of ligand to the latter induces a conformational change to a high affinity state ($Rb'N$). This model is also untenable, since it predicts that the rate of dissociation cannot exceed the isomerization rate (i.e., $Rb'N \rightarrow RbN$) which is rate-limiting for dissociation. However, the present data show that the off-rate (k_6) is about 3-fold higher than the isomerization rate constant ($k_e = k_7 + k_8$) at low nicotine concentrations (Table

TABLE 2

Effects of membrane properties on kinetic parameters

Whole brain membrane preparations, P-2 fractions, and synaptosomes were prepared as described under Materials and Methods. Association kinetics were monitored by incubating membranes (0.25 mg of protein) with 2 nM ^{3}H-L-nicotine for varying amounts of time (0–2 hr) at 0°. The rate of dissociation was determined by isotopic dilution of equilibrated samples (0°, 2 hr) with unlabeled L-nicotine salicylate (1 mM). Blank incubations contained 100 μM L-nicotine salicylate. Kinetic rate constants were determined as described in the text. The results shown are representative of at least two experiments, performed in triplicate.

Membrane preparation	Rate constant		
	Association (k_{ob})	Dissociation	Isomerization (k_e)
		min^{-1}	
Whole brain	0.08	0.04	0.016
Permeabilized membranes[a]	0.06	0.04	0.020
P-2 fraction	0.08	0.04	0.017
Synaptosomes	0.07	0.05	0.017

[a] Membrane preparations from whole brain were incubated with 0.5 mg/ml saponin on ice for 1 hr before incubations with radiolabeled ligand were initiated.

TABLE 3

Effects of temperature on kinetic parameters

Membranes (0.25 mg of protein) were incubated with 2 nM ^{3}H-L-nicotine for varying amounts of time at 0°, 22°, or 37°. Blank incubations contained 100 μM L-nicotine salicylate. Kinetic rate constants were estimated as described in the text.

Temperature	Rate constant		
	Association (k_{ob})	Dissociation	Isomerization (k_e)
		min^{-1}	
0	0.08	0.04	0.016
22	0.70	0.40	0.280
37	1.50	0.84	0.530

1). Furthermore, in order to observe first order dissociation under all conditions (Fig. 5), the isomerization rate would have to be identical to the off-rate for the high affinity sites ($RaN \rightarrow Ra + N$) which would be highly fortuitous.

A more complex model than the two-state model was also considered. It is based on the formation of diliganded receptors, and was proposed by Prinz and Maelicke (27) to account for the binding properties of purified nicotinic cholinergic receptors from *Electrophorus*.

$$R + N \leftrightarrow RN \leftrightarrow NRN$$

$$R'N \leftrightarrow NR'N$$

Unfortunately, because of the experimental error limits (ca. ±5%) associated with the filtration assay, the additional kinetic parameters associated with this model were not measurable in the present studies. Therefore, this model could not be distinguished experimentally from the two-state model and cannot be ruled out as a possible alternative. However, it is interesting to note that one prediction of the model is that the rate of dissociation, as measured by the addition of competing ligand, is decelerated at higher concentrations of the chasing ligand (27). This phenomenon was not observed in the present studies, which may be an indication of subtle differences between peripheral nicotinic receptors and those in the brain.

The present results invite comparison with studies on peripheral nicotinic cholinergic receptor systems where a two-state model has also been applied. For example, Boyd and Cohen (28) used a filtration assay to study the kinetics of [^{3}H]acetylcholine binding to *Torpedo* postsynaptic membranes. The results were analyzed in terms of a two-state mechanism. Their data were consistent with a high affinity conformer (K_d = 1 nM) that accounted for 20% of the total sites in the absence of ligand and a low affinity conformer with a K_d of 500 nM. Based on the present studies, the properties of nicotine-binding sites in the mammalian brain appear to be surprisingly similar. The apparent affinities of the high and low affinity conformers, with K_d = 1 nM and 150 nM, respectively, compare reasonably well with those determined for acetylcholine binding in *Torpedo* tissue. The apparent equilibrium dissociation constant (K_{eq}) for nicotine binding (2–3 nM) is slightly lower than that determined for acetylcholine (8 nM) and the percentage of sites represented by the high affinity conformer was found to be somewhat higher (40%) in rat brain membranes. Conversely, the absolute kinetic rate constants determined in the present studies are significantly lower than those reported for either *Torpedo* membranes (28) or for the purified acetylcholine receptor from *Electrophorus* (27), by 1 to 2 orders of magnitude. In general, lower rates of association and dissociation appear to be typical for the binding of acetylcholine and nicotine to membranes from mammalian brain tissue (9, 10). This led us to explore the possibility that this phenomenon might be reflecting the heterogeneity of the preparations or the presence of rate-limiting diffusion barriers, such as outside-in membrane vesicles or postsynaptic elements. However, based on the data of Table 2, these possibilities seem unlikely. Therefore, the discrepancies may simply be due to methodological differences.

Some interesting comparisons can also be made with other studies where the kinetics of agonist binding to brain membrane preparations have been monitored. For example, Sloan *et al.* (36) showed that [^{3}H]nicotine binding to P-2 membrane fractions was biphasic. The present results are in agreement with this observation. In contrast, the data of Schwartz *et al.* (9) gave no indication of a similar phenomenon for [^{3}H]acetylcholine binding. These differences present an interesting dilemma in view of the fact that both ligands bind to sites in the brain with high affinity. A possible explanation may be that acetylcholine is a relatively less stable ligand. In our hands it was difficult to assess the true equilibrium point for [^{3}H]acetylcholine binding because of a slow decrease in specific binding between 1 and 3 hr, even in the presence of physostigmine (data not presented). This point will need to be clarified in order to gain a better understanding of how these ligands interact with receptor sites in the brain.

In general, the two-state model appears to be adequate for describing the properties of nicotinic binding sites at physiological temperatures. For example, the apparent affinity of the sites, calculated from the kinetic data, did not change appreciably at higher temperatures. By comparison, the results of Table 3 indicate that the increase in the isomerization rate (k_s) with temperature is proportionally higher than either the association or dissociation rates. This finding suggests that the molecular properties of the sites which determine the conformational equilibria may be more sensitive to temperature effects. At 37° the process of isomerization is quite rapid. The data of Table 3 suggest a half-time of around 1 min. However, this rate was measured at relatively low ligand concentrations (2 nM) and therefore reflects the rate of "relaxation" ($k_7 + k_8$) of the high affinity to the low affinity conformer ($R' \rightarrow R$) upon removal of agonist (28). As such it should be considered a minimal estimate of the rate of the ligand-induced conformational transition ($RN \rightarrow R'N$) that would occur at saturating concentrations of nicotine. It is tempting to speculate that these conformational transitions are related to the process of receptor desensitization *in vivo*. If this is the case, then desensitization would occur rapidly at physiological temperature (i.e., within minutes) and be freely reversible. However, at this point the predictive value of the two-state model with respect to receptor function remains to be tested.

Acknowledgments

We express our appreciation to Dr. Thomas Perfetti for the preparation of L-nicotine salicylate and to Ms. Regina Watkins Brim for preparation of the manuscript.

References

1. Raftery, M. A., B. M. Conti-Tronconi, S. M. J. Dunn, R. D. Crawford, and D. Middlemas. The nicotinic acetylcholine receptor: its structure, multiple binding sites, and cation transport properties. *Fund. Appl. Toxicol.* **4**:S34–S51 (1984).
2. Dolly, J. O., and E. A. Barnard. Nicotinic acetylcholine receptors: an overview. *Biochem. Pharmacol.* **33**:841–858 (1984).
3. Changeaux, J. P., A. Devillers-Thiery, and P. Chemouilli. Acetylcholine receptor: an allosteric protein. *Science (Wash. D. C.)* **225**:1335–1345 (1984).
4. Maelicke, A. Biochemical aspects of cholinergic excitation. *Angew. Chem. Int. Ed. Engl.* **23**:195–221 (1984).
5. Schmidt, J. Drug binding properties of an α-bungarotoxin-binding component from rat brain. *Mol. Pharmacol.* **13**:283–290 (1977).
6. Duggan, A. W., J. G. Hall, and C. Y. Lee. Alpha-bungarotoxin, cobra neurotoxin and excitation of Renshaw cells by acetylcholine. *Brain Res.* **170**:166–170 (1976).
7. Ko, C. P., H. Burton, and R. P. Bunge. Synaptic transmission between rat spinal cord explants and dissociated cervical ganglion neurons in tissue culture. *Brain Res.* **117**:437–460 (1976).
8. Carbonetto, S. T., D. M. Fambrough, and K. J. Muller. Nonequivalence of α-bungarotoxin receptors and acetylcholine receptors in chick sympathetic neurons. *Proc. Natl. Acad. Sci. USA* **75**:1016–1020 (1978).
9. Schwartz, R. D., R. McGee, Jr., and K. J. Keller. Nicotinic cholinergic receptors labeled by [^{3}H]acetylcholine in rat brain. *Mol. Pharmacol.* **22**:56–62 (1982).
10. Marks, M. J., and A. C. Collins. Characterization of nicotine binding in

mouse brain and comparison with the binding of α-bungarotoxin and quinuclidinyl benzilate. *Mol. Pharmacol.* **22**:554–564 (1982).
11. Abood, L. G., S. Grassi, and M. Costanza. Binding of optically pure (−)-[^{3}H]nicotine to rat brain membranes. *FEBS Lett.* **157**:147–149 (1983).
12. Lippiello, P. M., and K. G. Fernandes. The binding of L-[^{3}H]nicotine to a single class of high affinity sites in rat brain membranes. *Mol. Pharmacol.* **29**:448–454 (1986).
13. Clarke, P. B. S., R. D. Schwartz, S. M. Paul, and C. B. Pert and A. Pert. Nicotinic binding in rat brain: autoradiographic comparison of [^{3}H]acetylcholine, [^{3}H]nicotine, and [^{125}I]-α-bungarotoxin. *J. Neurosci.* **5**:1307–1315 (1985).
14. Sugiyama, H., and Y. Yamashita. Characterization of putative nicotinic acetylcholine receptors solubilized from rat brains. *Brain Res.* **373**:22–26 (1986).
15. Wonnacott, S. α-Bungarotoxin binds to low-affinity nicotine binding sites in rat brain. *J. Neurochem.* **47**:1706–1712 (1986).
16. Martino, A. M., V. Hamui, and K. J. Kellar. [^{3}H]Acetylcholine and [^{3}H](−)nicotine label the same nicotinic cholinergic binding site in brain. *Soc. Neurosci. Abstr.* **11**:93 (1985).
17. Marks, M. J., J. A. Stitzel, E. Romm, J. M. Wehner, and A. C. Collins. Nicotinic binding sites in rat and mouse brain: comparison of acetylcholine, nicotine, and α-bungarotoxin. *Mol. Pharmacol.* **30**:427–436 (1986).
18. Romano, C., and A. Goldstein. Stereospecific nicotine receptors on rat brain membranes. *Science (Wash. D. C.)* **210**:647–650 (1980).
19. Schwartz, R. D., and K. J. Kellar. Nicotinic cholinergic receptor binding sites in the brain: regulation *in vivo*. *Science (Wash. D. C.)* **220**:214–216 (1983).
20. Marks, M. J., J. B. Burch, and A. C. Collins. Effects of chronic nicotine infusion on tolerance development and nicotinic receptors. *J. Pharmacol. Exp. Ther.* **226**:817–825 (1983).
21. Schwartz, R. D., J. Lehmann, and K. J. Kellar. Presynaptic nicotinic cholinergic receptors labeled by [^{3}H]acetylcholine on catecholamine and serotonin axons in brain. *J. Neurochem.* **42**:1495–1498 (1984).
22. Clarke, P. B. S., and A. Pert. Autoradiographic evidence for nicotinic receptors on nigrostriatal and mesolimbic dopaminergic neurons. *Brain Res.* **348**:355–358 (1985).
23. Giorguieff-Chesselet, M. F., M. L. Kemel, D. Wandscheer, and J. Glowinski. Regulation of dopamine release by presynaptic nicotinic receptors in rat striatal slices: effect of nicotine in a low concentration. *Life Sci.* **25**:1257–1262 (1979).
24. Brown, D. A. Neurotoxins and the ganglionic (C6) type of receptor. *Adv. Cytopharmacol.* **3**:225–230 (1979).
25. Abood, L. G., D. T. Reynolds, and J. M. Bidlack. Stereospecific ^{3}H-nicotine binding to intact and solubilized rat brain membranes and evidence for its noncholinergic nature. *Life Sci.* **27**:1307–1314 (1980).
26. Galper, J. B., W. Klein, and W. A. Catterall. Muscarinic acetylcholine receptors in developing chick heart. *J. Biol. Chem.* **252**:8692–8699 (1977).
27. Prinz, H., and A. Maelicke. Interaction of cholinergic ligands with purified acetylcholine receptor protein. *J. Biol. Chem.* **258**:10273–10282 (1983).
28. Boyd, N. D., and J. B. Cohen. Kinetics of binding of [^{3}H]acetylcholine and [^{3}H]carbamoylcholine to *Torpedo* post synaptic membranes: slow conformational transitions of the cholinergic receptor. *Biochemistry* **19**:5344–5353 (1980).
29. Whittaker, V. P., and L. A. Barker. The subcellular fractionation of brain tissue with special reference to the preparation of synaptosomes and their component organelles. *Methods Neurochem.* **2**:1–52 (1972).
30. McCarthy, K. D. An autoradiographic analysis of beta adrenergic receptors on immunocytochemically defined astroglia. *J. Pharmacol. Exp. Ther.* **226**:282–290 (1983).
31. Lowry, O. H., N. J. Rosebrough, A. L. Farr, and R. J. Randall. Protein measurement with the Folin phenol reagent. *J. Biol. Chem.* **193**:165–175 (1951).
32. Munson, P. J., and D. Rodbard. LIGAND: a versatile computerized approach for characterization of ligand-binding systems. *Anal. Biochem.* **107**:220–239 (1980).
33. Katz, B., and S. Thesleff. A study of the "desensitization" produced by acetylcholine at the motor end-plate. *J. Physiol. (Lond.)* **138**:63–80 (1957).
34. Perfetti, T. A. Structural study of nicotine salts. *Beitr. Tabakforsch. Int.* **12**:43–54 (1983).
35. Lancet, D., and I. Pecht. Kinetic evidence for hapten-induced conformational transition in immunoglobulin MOPC 460. *Proc. Natl. Acad. Sci. USA* **73**:3549–3553 (1976).
36. Sloan, J. W., G. D. Todd, and W. R. Martin. Nature of nicotine binding to rat brain P_2 fraction. *Pharmacol. Biochem. Behav.* **20**:899–909 (1984).

Send reprint requests to: Dr. P. M. Lippiello, Bowman Gray Technical Center, Building 611-13, Room 104W, R. J. Reynolds Tobacco Company, Winston-Salem, NC 27102.